International Journal of Artificial Intelligence, Machine Learning and Data Analytics
www.ijaimda.org

| **Open Access** |

Integrated Computational Retinal Vascular Morphometry Using Fractal, Skeleton-Based, and Phi-Related Features for Diabetic Retinopathy and Glaucoma.

Ahed J Alkhatib

Department of Legal Medicine, Toxicology and Forensic Medicine, Jordan University of Science & Technology, Jordan ajalkhatib@just.edu.jo (retired).
ORCID: https://orcid.org/0000-0003-3359-8128
Corresponding Author: Ahed J Alkhatib, ajalkhatib@just.edu.jo

ARTICLE INFO

Article History:

Received 05/06/2026
Revised 30/06/2026
Accepted 13/07/2026

CITE AN ARTICLE:

Alkhatib A. J., (2026). ***Integrated Computational Retinal Vascular Morphometry Using Fractal, Skeleton-Based, and Phi-Related Features for Diabetic Retinopathy and Glaucoma****. International Journal of Artificial Intelligence, Machine Learning and Data Analytics, 1(1), 43-50*
https://www.ijaimda.org/index.php/ijaimda/article/view/3

ABSTRACT

Background: Fundus images can be used to quantify retinal vascular morphology using density, fractal and graph-based metrics. Exploratory work with phi-related proportional indices is most commonly incomplete or there are no real-world reports.
Objective: To assess whether the global vascular morphology, fractal complexity, skeleton topology, and phi-derived proportional features of healthy, diabetic retinopathy, and glaucoma eyes are different in the HRF dataset.
Methods: Out of 45 HRF fundus images analyzed, 15 each were healthy, diabetic retinopathy, and glaucoma with expert matched vessel and field-of-view masks. Global features included vessel density, edge density, fractal dimension, lacunarity, ratios of regional densities, and phi-deviation indices. The skeletons in downsampled vessels utilized at branch level so that the subsequent features are extracted from the skeleton length of the vessel, endpoint of the vessel, cluster of the branches, ratio of the segments, geo-metric tortuosity proxies, branch phi-deviation features. Differences in group characteristics using permutation ANOVA with 5,000 permutations were investigated. Moreover, the use of a leave-one-out nearest-centroid model was explored.
Results: Healthy retinas showed higher vessel density and fractal dimension, whereas diabetic retinopathy and glaucoma showed higher lacunarity. Skeleton analysis showed higher skeleton length and branch-cluster density in healthy eyes, while disease groups showed much higher endpoint density and endpoint/branch-cluster ratios. Integrated global morphology plus skeleton features achieved 84.4% exploratory classification accuracy.
Conclusion: Morphometric differences linked to diseases were captured using fractal and skeleton techniques in the HRF dataset. Indices related to phi must be considered exploratory descriptors, rather than bona fide biomarkers.

Keywords **-** Retinal Fundus Imaging; Fractal Dimension; Vascular Skeleton; Diabetic Retinopathy; Glaucoma; Golden Ratio; Morphometry.

1. INTRODUCTION

The retinal microvasculature is visible extension of the central nervous system (CNS) and circulatory system (CS) and provides an opportunity to study the human CNS and CS non-invasively via fundus photograph (Shi et al., 2025). This accessibility has ensured that this modality has emerged as a valuable platform for computational morphometry of retinal structures in diseases where microvascular integrity, vessel distribution and vascular topology have biological meaning (Agrawal et al., 2025). The disease manifestation in diabetic retinopathy is retinal vascular alteration (Reddy et al., 2024). In glaucoma, there are vascular contributions but they are less direct and still relevant clinically (Mursch-Edlmayr et al., 2021). It was shown that the caliber, perfusion, fractal dimension, tortuosity and branching geometry are associated with the optic nerve and retinal nerve fiber layer changes. (Sng et al., 2018).

Fractal analysis is appealing because the retinal vascular tree has a branching, scale-dependent structure (Masters, 2004). Fractal dimension gives a concise estimate of the density of a vascular pattern in space in a measurement scale (Esteban and Vargas, 2026). Yu and Lakshminarayanan (2021) conducted a meta-analysis that found promising diagnostic relevance for retinal fractal dimension, but demonstrated variation between imaging protocols, segmentation methods, and analytic pipelines. Likewise, retinal fractal dimension is suggested by Lemmens et al (2020) as a candidate biomarker in neurovascular and neurodegenerative conditions but they emphasize the need of methodology standardization and interpretation caution.

Apart from the fractal dimension, it is possible to study the vessel tree as a topology of endpoints, bifurcations and connecting segments by graph and network representations (Shang et al., 2026). The work of Amil et al. (2019) indicates that the strength of network-based vessel features can distinguish between healthy, diabetic retinopathy and glaucoma images. Results are sensitive to the image resolution and segmentation method (Shang et al., 2026). It is the most relevant study to the present study as it studied HRF images and proved the usefulness of skeletonized and graph-like vascular representations. In other words, branch-level topology must complement the features of global density and fractals, argue the authors (Hartley et al., 2024).

Phi is a different concept, compared to the golden ratio (Pehlivan et al., 2026). The ratio is a true mathematical ratio, but its translation into the biological and medical domains is often overextended (Naini, 2024). Studies on facial and surgical proportion reveal that claims of golden-ratio should be treated with caution and (not) taken as universal biological rules (Hwang and Park, 2021; Londono et al., 2024). Consequently, phi was not used as a diagnostic law in this study. The phi-deviation variables were defined as exploratory proportional descriptors of regional vascular balance and branch-length distribution instead. By framing phi in this way allows it to be tested as a mathematical descriptor and does not claim universal life harmony.

The current experiment utilized the HRF fundus image dataset (from high-resolution retinal vessel segmentation research by Odstrcilik et al (2013) for the comparison of healthy, diabetic retinopathy and, glaucoma eyes. The purpose was to find out whether the global morphometry, fractal architecture, skeleton topology and phi-related proportional features offer complementary information about the retinal vascular structure.

2. METHODS

Dataset and Study Design

A secondary image-analysis study was conducted using the HRF segmentation dataset. The uploaded archive contained 45 high-resolution fundus images of 15 healthy, 15 diabetic retinopathy, and 15 glaucoma eyes. Each image was given an expert vessel segmentation mask and field-of-view mask. The HRF dataset is appropriate for this pilot due to its disease-group labels and manual vessel segmentations. This allows morphometric values to be extracted from the expert masks directly, rather than needing to train incorrect segmentation models (Odstrcilik et al., 2013) (Figure 1).

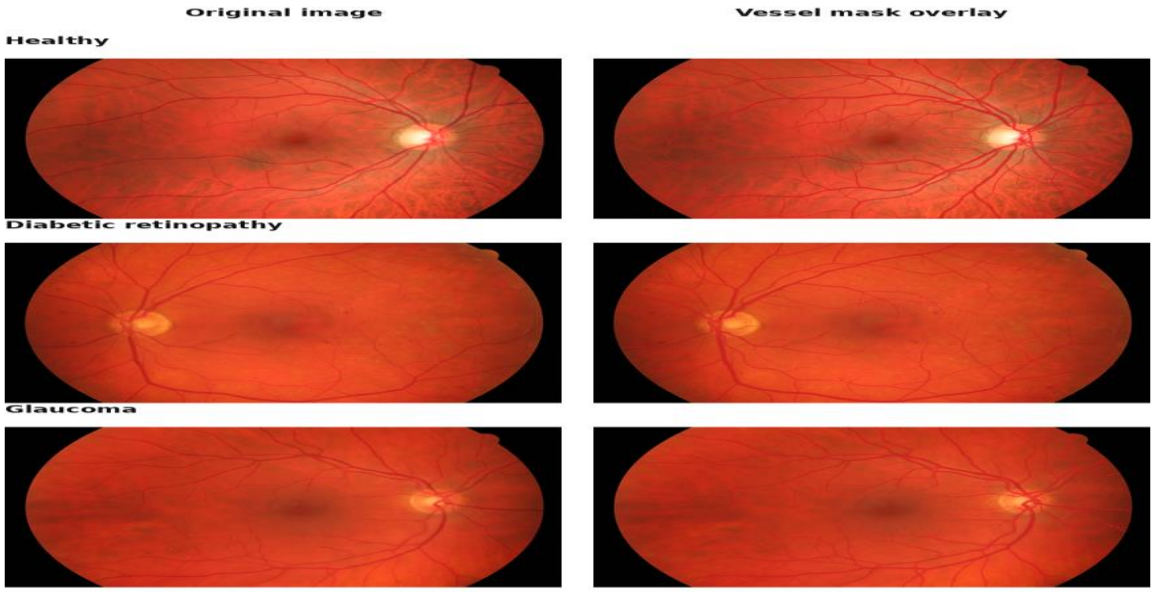

Figure 1: Representative original fundus images and vessel-mask overlays from the HRF dataset.

Global Vascular, Fractal, and Regional Features

All measurements used the mask of the focal retina. The global density of blood vessels as the total pixels identified as vessel in the field of view. The author of the paper used edge-density to simply indicate the boundary complexity. From the binary vessel mask, box-counting fractal dimension was calculated to estimate scale-dependent vascular occupancy while lacunarity was calculated to reflect spatial heterogeneity (or gappiness) in the vascular pattern. Retinal vascular complexity features are similar to those identified in previous work examining disease effects on ocular and systemic disease, although imaging and segmenting choices influence estimates (Yu and Lakshminarayanan, 2021).

Based on regional features, we can classify the field into central, middle, peripheral, upper, lower, left, right and quadrant regions. Ratios were derived for central/peripheral, central/middle, upper/lower, left/right, and quadrants. Phi-deviation indices were calculated by comparing normalized ratios with phi. Prior to calculating deviation, we inverted all ratios under 1, so that the (Phi) variables indicate distance from the golden ratio and not direction of imbalance. This viewing of phi is as formal proportion reference and not biological optimum.

Skeleton and Branch-Level Features

To perform branch-level analysis, the vessel masks were downsampled four-times and then skeletonized using a Zhang-Suen thinning algorithm. To ensure the pipeline could be reproduced effectively and efficiently, downsampling was used which results the features of the skeleton can be interpreted as relative group level indices rather than full-resolution clinical measurements. We extracted skeleton length density, endpoint density, branch-cluster density, ratios of endpoint/branch-cluster, segment number, ratios of segment-length distributions, segment-length ϕ-deviation indices and tortuosities proxies. The design depicts graph-based logic, where endpoints and bifurcations function as nodes and the paths of vessels appear as connecting segments (Amil et al., 2019).

Statistical and Classification Analysis

We screened the group differences using permutation ANOVA with 5000 label permutations. This method was selected due to the limited sample size and exploratory character of the feature set. Leave-one-out nearest-centroid models were used for classification assessment. These models were deliberately simple and were only used to test whether feature families carried group-separating information. They were not intended to be clinical diagnostic tools.

3. RESULTS

Global Fractal and Proportional Morphometry

As illustrated in Table (1) and Figure (2), retinal vascular architecture varies significantly between healthy and diseased images. Every one of the variables listed has a p-value of less than 0.001 indicating that all three groups differ significantly for each measured parameter.

Vessel density was recorded highest in healthy eyes: 0.110 ± 0.011, 0.082 ± 0.012 were reported in healthy and diabetic retinopathy and 0.082 ± 0.007 in glaucoma. The healthy retina had a more prominent visible vascular network, while the two disease groups had a reduction in vessel coverage in the retinal field.

Healthy eyes exhibited the highest Fractal dimension of 1.484 ± 0.021. Also, in diabetic retinopathy, it was 1.435 ± 0.032 and glaucoma, 1.438 ± 0.019. The fact that the fractal dimension reflects the overlapping and richness of vascular branching suggests a disease that is less complex in the retina.

The pattern exhibited by lacunarity was opposite. The value was observed lowest in healthy eyes with the value of 1.669 ± 0.045. It was higher in diabetic retinopathy with a value of 1.882 ± 0.104. There was slightly lower value in glaucoma with 1.831 ± 0.044. A higher lacunarity indicates that the vascular network has bigger gaps and more irregular spacing or heterogeneity. Diseased retinas exhibit greater spatial irregularity and fragmentation.

In diabetic retinopathy, this central/peripheral ratio was reduced to 0.681 ± 0.156 compared to healthy eyes 0.933 ± 0.064 and glaucoma 0.926 ± 0.126. The findings imply a comparatively greater reduction in central vascular density for diabetic retinopathy than peripheral vascular density. Glaucoma showed a central/peripheral distribution closer to healthy eyes overall despite lower density.

The middle/center ratio followed the same trend. The highest was healthy eye with 0.631 ± 0.048, the lowest diabetic retinopathy with 0.459 ± 0.087 and glaucoma was intermediate with 0.583 ± 0.076. This signifies again that diabetic retinopathy has the highest disturbance of vascular proportionality amid retinal zones.

The greatest coefficient of variation in quadrants was seen in diabetic retinopathy values: 0.251 ± 0.053 in diabetics, followed by 0.159 ± 0.041 in healthy eyes and 0.184 ± 0.043 in glaucoma. More uneven evenly distribution of vessel density in retinal quadrants was indicated by the higher coefficient of variation. Consequently, the most asymmetric or uneven vascular distribution was diabetic retinopathy.

The central middle deviation phi was the least in healthy eyes: 0.098 ± 0.070 whereas the highest was in diabetic retinopathy: 0.651 ± 0.425. Lower phi deviation indicates closer correspondence with the chosen reference proportion relative to phi. This finding suggests that healthy retinas closely correspond with the proposed phi-related proportion for the vasculature. Subject with glaucoma had a moderate phi deviation, while diabetic retinopathy exhibited the greatest disruption in proportion.

Table 1: Global vascular, fractal, and phi-related feature summaries.

Feature	Healthy	Diabetic retinopathy	Glaucoma	p
Vessel density	0.110 +/- 0.011	0.082 +/- 0.012	0.082 +/- 0.007	<0.001
Fractal dimension	1.484 +/- 0.021	1.435 +/- 0.032	1.438 +/- 0.019	<0.001
Lacunarity	1.669 +/- 0.045	1.882 +/- 0.104	1.831 +/- 0.044	<0.001
Central/peripheral ratio	0.933 +/- 0.064	0.681 +/- 0.156	0.926 +/- 0.126	<0.001
Central/middle ratio	0.631 +/- 0.048	0.459 +/- 0.087	0.583 +/- 0.076	<0.001
Quadrant density CV	0.159 +/- 0.041	0.251 +/- 0.053	0.184 +/- 0.043	<0.001
Phi deviation: central/middle	0.098 +/- 0.070	0.651 +/- 0.425	0.203 +/- 0.125	<0.001

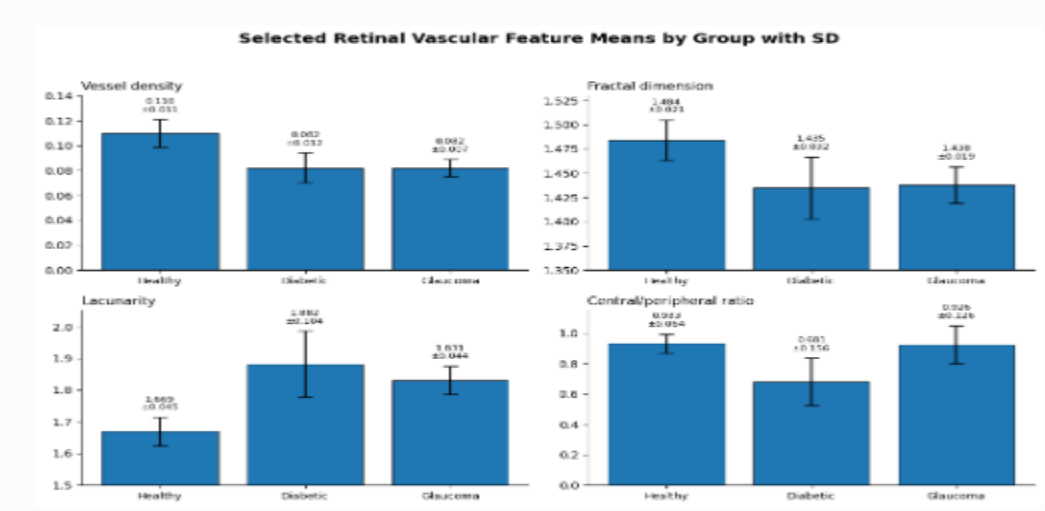

Figure 2: Selected global vascular and proportional feature means by group.

Branch-Level Skeleton Morphometry

According to Table (2) and Figure (3), the skeletons and branches of retinal vessel architectures are *distinct* in healthy, diabetic retinopathy, and glaucoma images. By transforming the vessel mask into a thin skeleton, we can interpret the vascular network. ClassyFIER will compute vessel length, endpoints, branch clusters, segment structure and tortuosity.

The healthy retinas had the highest skeleton length density; the diabetic retinopathy had a lower density whereas the glaucoma had an intermediate density. The difference was significant ($p = 0.012$), indicating that healthy retinae preserved a longer and more continuous vascular skeleton in the retinal field.

The endpoint density demonstrated the greatest group separation. There were far fewer endpoints in healthy retinas: 84.311 ± 21.115 per 100k FOV pixels as compared to diabetic retinopathy (278.486 ± 52.964) and glaucoma (299.557 ± 50.747) ($p < 0.001$). If endpoint density is high, the junctions are disturbed or fragmented. As a result, both disease groups had a less constant vascular tree.

According to the study results, the healthy eyes had highest branch-cluster density of 221.287 ± 20.30 and lower density of diabetic retinopathy (DR) 173.128 ± 34.677 and glaucomatous eyes 182.183 ± 27.37 ($p < 0.001$) respectively. Healthy retina had more branched organizations while diseased retina had fewer branched clusters.

The ratio of the endpoint or branch clusters effectively differentiated between healthy and diseased eyes. The ratio was significantly lower in healthy retinal tissues (0.379 ± 0.082) as compared with diabetic retinopathy (1.655 ± 0.366) and glaucoma (1.670 ± 0.333) ($p < 0.001$). In disease, endpoints became more frequent relative to branch points, suggesting that the disease pathology is consistent with vascular rarefaction, pruning or segmentation fragmentation.

The ratio of segment length to the average of the quartiles (q75/q25) was slightly bigger for the healthy retinas: 3.847 ± 0.388 compared with 3.612 ± 0.297 in diabetes retinopathy, and 3.535 ± 0.311 in glaucoma ($p = 0.043$). Our findings imply that vascular trees that are healthy have a greater distribution of segment-lengths whereas diseased groups have a slight decrease.

The highest segment of the phi deviation q75/q25 was for healthy eyes: 2.229 ± 0.388, while it was lower for diabetic retinopathy: 1.994 ± 0.297 and lowest for glaucoma: 1.917 ± 0.311 ($p = 0.042$). At the branch level, the measured difference is statistically significant but modest. It ought to be interpreted cautiously as exploratory proportional descriptor rather than confirmed biological marker.

In the end, mean segment tortuosity was the highest in healthy retinas; 1.057 ± 0.003; lower in diabetic retinopathy 1.051 ± 0.003 and lowest in glaucoma 1.048 ± 0.002 ($p < 0.001$). In spite of any small absolute numerical differences, they are statistically significant. This might indicate slight variations in vessel curvature or geometry of skeletonized segments across groups.

In general, information in Table (2) supports the major finding that healthy retinas have a more continuous, branched and organized vascular skeleton compared to those affected by diabetic retinopathy and glaucoma which display a more fragmented vascular tree with more endpoints but less branch clusters greater endpoints to branch ratio. With respect to biological interpretability, the strongest features are endpoint density, branch-cluster density, and endpoint/branch-cluster ratio. The phi-related segment measure is of interest but should remain exploratory.

Table 2: Skeleton and branch-level feature summaries.

Feature	Healthy	Diabetic retinopathy	Glaucoma	p
Skeleton length density	0.062 +/- 0.007	0.053 +/- 0.009	0.056 +/- 0.007	0.012
Endpoint density per 100k FOV pixels	84.311+/- 21.115	278.486 +/- 52.964	299.56 +/- 50.75	<0.001
Branch-cluster density per 100k FOV pixels	221.287+/- 20.30	173.128 +/- 34.677	182.183+/- 27.37	<0.001
Endpoint/branch-cluster ratio	0.379 +/- 0.082	1.655 +/- 0.366	1.670 +/- 0.333	<0.001
Segment length q75/q25 ratio	3.847 +/- 0.388	3.612 +/- 0.297	3.535 +/- 0.311	0.043
Phi deviation: segment q75/q25	2.229 +/- 0.388	1.994 +/- 0.297	1.917 +/- 0.311	0.042
Mean segment tortuosity	1.057 +/- 0.003	1.051 +/- 0.003	1.048 +/- 0.002	<0.001

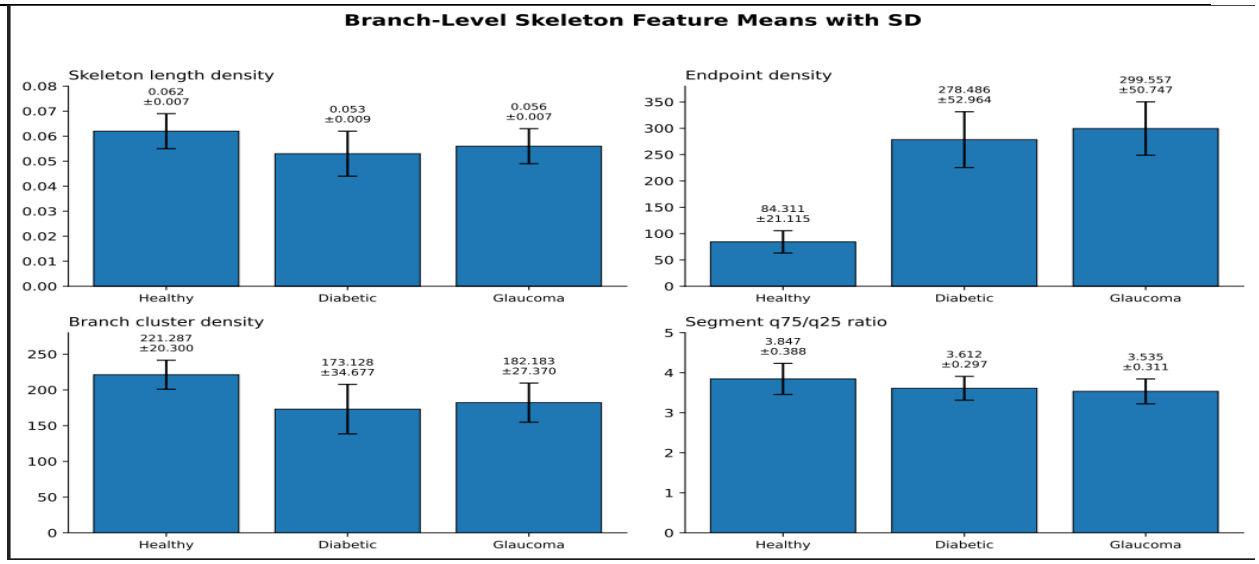

Figure 3: Selected branch-level skeleton feature means by group

Exploratory Classification

Data from Table (3) classify the images as healthy (H), diabetic retinopathy (DR), and glaucoma (G) using the leave-one-out nearest-centroid classifier. Leave-one-out cross-validation tests each image once while utilizing the rest of the images to define the respective group centroids. As a result, the accuracy detailed is exploratory internal and not external.

The Morphology Core model based on global vascular features including vessel density, fractal dimension, lacunarity, and regional density balance gives 77.8 % accuracy. The signal that has disease-related information is strong already in most cases.

The model's accuracy based on world phi-related ratios achieved 62.2% - the Phi Exploratory. For a three-class problem, this is higher than random chance but evidently weaker than the core morphology model. Phi-related ratios will not result in sound classification on their own.

The Combined model made use of the global morphology and global phi-related ratios, resulting in increasing accuracy up to 82.2%. This indicates that phi-related features could add additional information on top of stronger classic morphometric features.

The Skeleton Core model, which incorporates skeleton topology measures (including skeleton length, endpoints, branch clusters, and endpoint-to-branch ratios) achieved an accuracy of 77.8%. This performance is on par with that of the global morphology model. This indicates that skeleton-level organization is a meaningful descriptor of retinal disease status.

Using branch-level phi-related ratios alone, a Branch Phi model attained 66.7% accuracy. This model is better than the global phi-only model but still weaker morphological or skeleton topology. As a result, phi measures which are branch-level are informative but not dominant.

The most effective model was the Integrated Core with a combination of global morphology and skeleton topology: 84.4% accuracy. This means that worldwide vascular complexity and branch-level network architecture provides information that complements each other.

The Integrated Phi Enriched model which had phi related features along with global morphology and skeleton features achieved 84.4%. The accuracy did not improve beyond the Integrated Core model, so once the stronger morphology and skeleton variables were included, the phi features did not improve classification.

Table 3: Leave-one-out nearest-centroid classification accuracy by feature family

Model	**Feature family**	**LOOCV accuracy**
Morphology Core	Global morphology	77.8%
Phi Exploratory	Global phi-related ratios	62.2%
Combined	Global morphology + phi	82.2%
Skeleton Core	Skeleton topology	77.8%
Branch Phi	Branch phi-related ratios	66.7%
Integrated Core	Global morphology + skeleton	84.4%
Integrated Phi Enriched	Global morphology + skeleton + phi	84.4%

4. DISCUSSION

The analysis of this expanded pilot supports the central role of fractal and skeleton-based retinal vascular morphometry. Diabetic retinopathy and glaucoma were observed to have higher lacunarity, while healthy retinas exhibited greater vessel density and fractal dimension. Per Yu and Lakshminarayanan (2021), the fractal dimension may be a compact and potentially method-sensitive measure of vascular complexity and retinal vascular architecture changes in disease that are consistent with the variation in pathology involved.

The skeleton analysis enhanced the interpretation by moving analysis from area occupancy to network topology. In both disease groups, endpoint density and endpoint/branch-cluster ratio were significantly increased, whereas branch-cluster density was increased in healthy eyes. The diseases studied were primarily neurodegenerative diseases. They said that the branches of the vessels associated with diseases have terminals or disconnected structures compared to branching clusters. This topology based interpretation is consistent with earlier analysis of retinal vessels based on graph, which showed that information associated with endpoints, bifurcations and connection segments are informative about disease not conveyed by the standard area of vessels (Amil et al., 2019).

It is also important to note that some of the measures are similar in diabetes and glaucoma. The global vascular density and fractal dimension in the eyes were lower in both disease groups compared to healthy eyes. Similarly, both disease groups showed elevated endpoint density. Nonetheless, a particularly reduced central / peripheral ratio was shown in diabetic retinopathy, while glaucoma maintained a closer central / peripheral ratio to a healthy eye. Some features might segregate health from disease while others might cause disease-type discrimination, this indicates.

The significance of phi should stay notably modest. The idea of a golden ratio has long been utilized in thinking about proportions and aesthetics and generally morphological phenomena. An extensive systematic evaluation presented in the paper suggests that the gold proportion should not be treated as a universal explanation (Hwang and Park, 2021; Londono et al., 2024). In this study, phi-deviation measures were found to be no better than fractal or skeleton features, and did not help in improving the integrated classifier beyond morphology plus skeleton alone. As such, they are best defined as exploratory: they can give mathematically defined proportional descriptors, but they are not validated biomarkers.

One of the strongest contributions of this work is the integrated framework. Worldwide traits depict volume, complexity, dispersion, plus regional equilibrium. Skeleton features showcase topology, fragmentation, and branch organization. Proportions of ratios derived from Phi serve as a layer for generating hypotheses. This hierarchy is scientifically valuable as it halts the manuscript over-claiming phi but maintains the novelty of proportional morphometry testing in a retinal disease context.

Limitations

- The HRF dataset consists of very few images to be used for analysis. Each class has only about 15 images. Thus all statistical and classification results are exploratory.
- The analysis employed expert masks instead of raw-image segmentation. This helps reduce the variability of segmentations but limits generalizability to automated clinical workflows.
- Skeletonization was done on masks with four-fold downsamples; confirmation work should repeat this analysis at a higher resolution, and graph-extraction validation.
- The closest-centroid probers for classifiers had been used only as simple feature-family-probes and must not be interpreted as diagnostic machine-learning models.
- Experts conducted external validations using conventional network and fractal benchmarks to construct variables related to phi.
- The dataset lacks the clinical detail metadata such as severity, duration, visual acuity, intraocular pressure (IOP), or systemic vascular comorbidities.

5. CONCLUSION

In analysis of the fundus image dataset of HRF, it was found that fractal and skeleton-based retinal vascular morphometry differentiate healthy images from diabetic retinopathy and glaucoma images. The outcome of the analysis strengthened the skeleton topology of disease-associated pattern of fragmentations was estimated through comparison of 4 species such as that the endpoint density and endpoint branch-cluster ratio are higher in disease group. The phi-related proportional indices showed exploratory value, although they were generally weaker than conventional morphometric and skeleton features. A suitable conclusion suggests that integrated fractal- and skeleton-

based morphometry may yield useful computational descriptors of retinal vascular architecture. However, phi-derived measures should be treated as supplementary and hypothesis-generating.

REFERENCES

[1] Amil, P., Reyes-Manzano, C. F., Guzman-Vargas, L., Sendina-Nadal, I., & Masoller, C. (2019). Network-based features for retinal fundus vessel structure analysis. PLOS ONE, 14(7), e0220132. https://doi.org/10.1371/journal.pone.0220132

[2] Agrawal, L., Agrawal, P. K., Agrawal, S. S., Sonune, M. S., Kadu, R. K., Kulkarni, M. B., & Bhaiyya, M. (2026). AI-driven multimodal retinal imaging for early detection and risk stratification of vascular and neurodegenerative diseases. Graefe's archive for clinical and experimental ophthalmology = Albrecht von Graefes Archiv fur klinische und experimentelle Ophthalmologie, 10.1007/s00417-026-07273-6. Advance online publication. https://doi.org/10.1007/s00417-026-07273-6

[3] Esteban, F. J., & Vargas, E. (2026). Foundations and Clinical Applications of Fractal Dimension in Neuroscience: Concepts and Perspectives. AppliedMath, 6(1), 7. https://doi.org/10.3390/appliedmath6010007

[4] Hartley, R.J.L., Jayathunga, S., Morgenroth, J. et al. Tree Branch Characterisation from Point Clouds: a Comprehensive Review. Curr. For. Rep. 10, 360–385 (2024). https://doi.org/10.1007/s40725-024-00225-5

[5] Hwang, K., & Park, C. Y. (2021). The divine proportion: Origins and usage in plastic surgery. Plastic and Reconstructive Surgery Global Open, 9(2), e3419. https://doi.org/10.1097/GOX.0000000000003419

[6] Lemmens, S., Devulder, A., Van Keer, K., Bierkens, J., De Boever, P., & Stalmans, I. (2020). Systematic review on fractal dimension of the retinal vasculature in neurodegeneration and stroke: Assessment of a potential biomarker. Frontiers in Neuroscience, 14, 16. https://doi.org/10.3389/fnins.2020.00016

[7] Londono, J., Ghasmi, S., Lawand, G., Mirzaei, F., Akbari, F., & Dashti, M. (2024). Assessment of the golden proportion in natural facial esthetics: A systematic review. The Journal of Prosthetic Dentistry, 131(5), 804-810. https://doi.org/10.1016/j.prosdent.2022.04.026

[8] Masters B. R. (2004). Fractal analysis of the vascular tree in the human retina. Annual review of biomedical engineering, 6, 427–452. https://doi.org/10.1146/annurev.bioeng.6.040803.140100

[9] Mursch-Edlmayr, A. S., Bolz, M., & Strohmaier, C. (2021). Vascular Aspects in Glaucoma: From Pathogenesis to Therapeutic Approaches. International journal of molecular sciences, 22(9), 4662. https://doi.org/10.3390/ijms22094662

[10] Naini F. B. (2024). The golden ratio-dispelling the myth. Maxillofacial plastic and reconstructive surgery, 46(1), 2. https://doi.org/10.1186/s40902-024-00411-2

[11] Odstrcilik, J., Kolar, R., Budai, A., Hornegger, J., Jan, J., Gazarek, J., Kubena, T., Cernosek, P., Svoboda, O., & Angelopoulou, E. (2013). Retinal vessel segmentation by improved matched filtering: Evaluation on a new high-resolution fundus image database. IET Image Processing, 7(4), 373-383. https://doi.org/10.1049/iet-ipr.2012.0455

[12] Pehlivan, İ., Bulut, S., & Güney, E. (2026). An Investigation into the Interpretation of Pi (π) as the Arithmetic Mean of the Golden Ratio (ϕ) and the Feigenbaum Constant (δ). Chaos and Fractals, 3(1), 61-64. https://doi.org/10.69882/adba.chf.2026019

[13] Reddy, S. K., Devi, V., Seetharaman, A. T. M., Shailaja, S., Bhat, K. M. R., Gangaraju, R., & Upadhya, D. (2024). Cell and molecular targeted therapies for diabetic retinopathy. Frontiers in endocrinology, 15, 1416668. https://doi.org/10.3389/fendo.2024.1416668

[14] Shang, W., Hong, G., Keller, W. E., Morton, R. A., Zeboulon, P., Kenichi, T., Duan, X., Gould, D. B., & Kim, T. N. (2026). A Three-dimensional Analytical Framework for Retinal Microvasculature Reveals Layer-associated Vulnerability in Development and Neovascular Remodeling. bioRxiv : the preprint server for biology, 2026.03.16.711909. https://doi.org/10.64898/2026.03.16.711909

[15] Shi, Q., Ni, A., Li, K., Su, W., Xie, W., Zheng, H., Wang, M., Xiao, Z., Wu, W., Shi, K., Zhang, P., Yan, B., Ding, D., Kwok, T., Zhao, Q., & Zhang, J. (2025). Retinal vascular alterations in cognitive impairment: A multicenter study in China. Alzheimer's & dementia : the journal of the Alzheimer's Association, 21(2), e14593. https://doi.org/10.1002/alz.14593

[16] Sng, C. C. A., Sabanayagam, C., Lamoureux, E. L., Liu, E., Lim, S. C., Hamzah, H., Lee, J., Tai, E. S., & Wong, T. Y. (2018). Retinal vasculature in glaucoma: A review. BMJ Open Ophthalmology, 3(1), e000032. https://doi.org/10.1136/bmjophth-2016-000032

[17] Van Eijgen, J., Fhima, J., Billen Moulin-Romsee, M. I., Behar, J. A., Christinaki, E., & Stalmans, I. (2024). Leuven-Haifa High-Resolution Fundus Image Dataset for Retinal Blood Vessel Segmentation and Glaucoma Diagnosis. Scientific Data, 11, 257. https://doi.org/10.1038/s41597-024-03086-6

[18] Yu, S., & Lakshminarayanan, V. (2021). Fractal dimension and retinal pathology: A meta-analysis. Applied Sciences, 11(5), 2376. https://doi.org/10.3390/app11052376